Modeling the low-voltage regime of organic diodes: Origin of the ideality factor

Chang Hyun Kim, Omid Yaghmazadeh, Yvan Bonnassieux, Gilles Horowitz

AIP | Journal of Applied Physics

Modeling the low-voltage regime of organic diodes: Origin of the ideality factor

Chang Hyun Kim, Omid Yaghmazadeh, Yvan Bonnassieux, and Gilles Horowitz

Citation: J. Appl. Phys. **110**, 093722 (2011); doi: 10.1063/1.3660221
View online: http://dx.doi.org/10.1063/1.3660221
View Table of Contents: http://jap.aip.org/resource/1/JAPIAU/v110/i9
Published by the American Institute of Physics.

Modeling the low-voltage regime of organic diodes: Origin of the ideality factor

Chang Hyun Kim,[a] Omid Yaghmazadeh, Yvan Bonnassieux, and Gilles Horowitz
LPICM, Ecole Polytechnique, CNRS, 91128 Palaiseau, France

(Received 22 July 2011; accepted 6 October 2011; published online 14 November 2011)

This paper investigates the physics of single-layer organic diodes in the low-voltage regime. A simple analytical model is developed to describe the current-voltage characteristics of the device. At variance with what is often reported in the literature, the operating mechanism of the organic diode is closer to that of the p-n junction than that of the conventional Schottky diode. The influence of an exponential distribution of traps is also analyzed. Alongside a drastic reduction of the current at above-diffusion-potential regime, traps introduce a substantial ideality factor in the low-voltage current. Two-dimensional physically based simulations are carried out in order to ascertain the validity of our model. By including trap effects, device simulation could fairly fit the experimental data of the organic diodes made of vacuum-evaporated pentacene. © *2011 American Institute of Physics*. [doi:10.1063/1.3660221]

I. INTRODUCTION

With the rapid development of organic electronic devices, such as organic light-emitting diodes (OLEDs)[1,2] and organic photovoltaic cells (OPVs),[3–5] a specific model for organic diodes becomes a key feature for interpretation and prediction of the device operation. Up to now, most of the diode models were directed toward OLEDs[6] and thus focused on the high-voltage regime (at least few volts). This is due to the fact that the emission starts at the onset voltage that is well above the diffusion (i.e., built-in) potential V_d. At this regime, the current is mainly controlled by bulk properties of the semiconducting layer. By contrast, a different situation prevails in OPVs, in which the open-circuit voltage roughly corresponds to the built-in voltage, so that the operation voltage is below V_d.[7] At this low-voltage regime, current generally follows an exponential behavior that strongly reminds the conventional metal-semiconductor (Schottky) contact. This is the reason that the Schottky diode model is often invoked to explain the behavior of organic diodes.[3,8] However, this model is based on the presence of a "depletion region" that extends over a small part of the whole thickness of the (inorganic) semiconductor, which, in fact, makes its application to organic solids questionable.

Imperfection of the Schottky model for "organic" diodes is expectable when general device and material configuration are taken into consideration. First, the thickness of an organic layer is usually much lower (typically 100 nm) than that of a Si wafer (~0.7 mm). Next, organic semiconductors are, in general, unintentionally doped so that free carrier density is extremely low (typically less than 10^{14} cm^{-3}). From these two arguments, the expected depletion width is actually higher than the film thickness in most cases. As a consequence, the energy diagram of the organic diode should be described by the metal-insulator-metal (MIM) representation[9] without any "partial" depletion region. Evidence for such a statement was recently reported by our group through impedance analysis on pentacene-based diodes.[10]

Another important limitation in organic semiconductors is the presence of traps, with the exception of highly pure, defect-free organic crystals. Energetic distribution of traps is most often described as an exponential or Gaussian density of states (DOS) near the transport band edges.[11–13] The primary effect of this DOS is to substantially decrease the current under forward bias.

In a historical point of view, the model presented here is largely based on the work developed during the early days of solid-state electronics. At that period, semiconductors were treated as highly resistive materials, in which charge carriers mainly arise from the injection at the contact electrode[14–18] (hence, the appellation of "dielectric diode"). An archetypal work is that by Wright,[17] which deals with one-dimensional one-carrier current in a plane parallel structure with one ohmic (injecting) contact and one blocking contact. On the basis of a resolution of coupled Poisson's and drift-diffusion equations, it was shown that, at low forward bias, current predominantly occurs by carrier diffusion and exponentially increases with the applied voltage, while, at higher forward voltage, the predominant mechanism is carrier drift and current follows a space-charge-limited power law. Due to the blocking electrode, reverse current is negligibly small and high rectification ratio could be achieved.

In the present work, we propose a simple analytical model that accounts for the current flow at low voltage in an organic diode composed of a single organic layer sandwiched between two conductors with different work functions. It is shown that the resulting current fairly compares to the calculated current by a physically based device simulation using drift-diffusion equations and finite-element integration. In addition to a significant reduction of the current above the built-in potential, it is found that an exponential distribution of traps leads to an emergence of the ideality factor in the exponential regime (low-voltage regime). With the trap effects included in the simulation, we could

[a]Electronic mail: chang-hyun.kim@polytechnique.edu.

successfully fit the experimental data measured on vacuum-evaporated pentacene diodes.

II. ANALYTICAL MODEL

The model diode consists of an organic layer inserted between a high work function (hereafter designated as the anode) and a low work function (the cathode) electrode, with the following assumptions: (1) in the absence of electrodes, there are no free carriers inside the semiconductor (the organic semiconductor is fully depleted and behaves as a pure dielectric); (2) only one type of carrier (electrons or holes) are injected from both electrodes. In the remainder of the paper, we will assume that these charge carriers are holes (hole-only conduction), keeping in mind that the extension to the electron-only or even bipolar system is straightforward (in the latter instance, it suffices to sum up the electron and hole currents).

Because of the first assumption, it is expected that there is no band bending upon contacting the semiconductor to the electrodes. The energy diagram of the metal-insulator-metal (MIM) diode is illustrated in Fig. 1. This figure also qualitatively depicts the operation regimes of the diode.

It is worth clarifying here that the mobility can be considered as constant in the diode configuration without carrier density dependence on it. This assumption is supported by the comparison of the carrier-density-dependent mobility in diodes and transistors.[19] This work indicates that, because the carrier concentration in diodes is much lower, the mobility is low and practically constant, whereas the mobility in transistors is substantially higher and more dependent on the carrier density.

A. Ideal case: Semiconductor without traps

1. Diode at thermal equilibrium

In this first part, we justify the energy diagram adopted in Fig. 1. We start from the one dimensional Poisson's Eq. (1) and drift-diffusion Eq. (2).

$$\frac{\mathrm{d}F}{\mathrm{d}x} = \frac{qp(x)}{\varepsilon}, \tag{1}$$

$$j = qp\mu F - qD\frac{\mathrm{d}p}{\mathrm{d}x}. \tag{2}$$

Here, F is the strength of the electric field, x the spatial coordinate in the direction perpendicular to the electrodes ($x = 0$ at the anode), q the elementary charge, p the density of holes, ε the permittivity of the semiconductor, j the current density, μ the hole mobility, and D their diffusion coefficient.

A generalized relation between the diffusion coefficient and the mobility can be found in the seminal textbook by Ashcroft and Mermin.[20] Its low carrier density limit reduces to Einstein relation $D/\mu = kT/q$, where k is Boltzmann constant and T the absolute temperature. Several recent papers discussed the validity of this relation in the case of organic semiconductors.[21–23] In general, it was found that a deviation from Einstein relation occurs with increased disorder (as measured by the variance of a Gaussian density of states) and charge carrier concentration. Here, we will assume that the semiconductor is partially ordered (or polycrystalline) and the carrier concentration is low enough (undoped or unintentionally doped semiconductor). Under such circumstances, the Einstein relation can be safely adopted. However, we recognize that further investigation on this assumption would deserve additional work in the future.

From the Einstein relation and Eq. (1), Eq. (2) becomes

$$j = \varepsilon\mu\left(F\frac{\mathrm{d}F}{\mathrm{d}x} - \frac{kT}{q}\frac{\mathrm{d}^2F}{\mathrm{d}x^2}\right). \tag{3}$$

At equilibrium (no voltage applied), $j = 0$, leading to the differential equation

$$F\frac{\mathrm{d}F}{\mathrm{d}x} - \frac{kT}{q}\frac{\mathrm{d}^2F}{\mathrm{d}x^2} = 0, \tag{4}$$

which can be integrated once,

$$\left(\frac{q}{2kT}\right)^2F^2 - \frac{q}{2kT}\frac{\mathrm{d}F}{\mathrm{d}x} = g^2, \tag{5}$$

where g is an integration constant.

In the Boltzmann approximation, Eq. (6) defines a relationship between the density of holes and the potential,

$$p = p_0e^{-qV/kT}, \tag{6}$$

where $p_0 = N_ve^{-E_b/kT}$ is the density of holes at $x = 0$. Here, N_v is the effective density of states at the valence band edge and E_b the (anode) barrier height at the electrode-semiconductor interface.

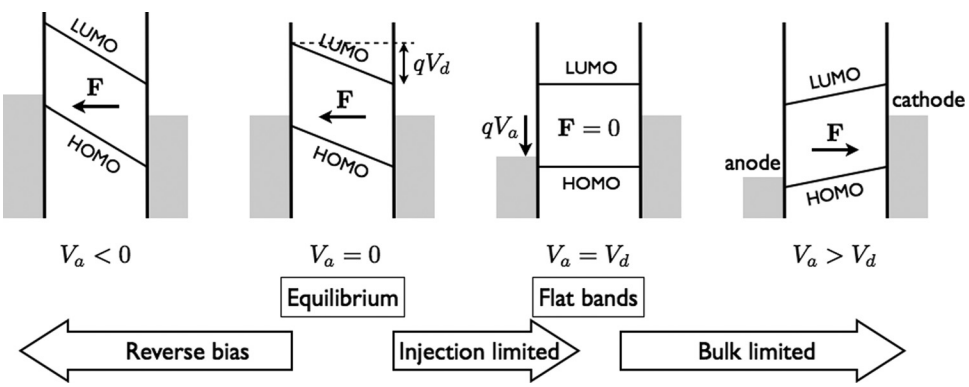

FIG. 1. Energy diagram of an MIM diode. V_d is the diffusion (or built-in) potential, which amounts to the difference between the work function of the anode and that of the cathode. V_a is the potential applied to the anode, with the cathode being connected to ground. From left to right: reverse-biased, thermal-equilibrium, flat-band, and forward-biased condition. The arrows symbolize the various regimes of the diode. From left to right: reverse bias, injection-limited forward bias, and bulk-limited forward bias regime.

Equation (5) was first resolved by Mott and Gurney for a semi-infinite semiconductor,[14] then by Skinner[24] for a semiconductor of finite thickness. The general solution writes

$$F(x) = -\frac{2kT}{q} g \coth g(x + x_1), \tag{7}$$

$$p(x) = \frac{2\varepsilon kT}{q^2} \frac{g^2}{\sinh^2 g(x + x_1)} = p_0 \left[\frac{gx_0}{\sinh g(x + x_1)}\right]^2, \tag{8}$$

where x_1 is an integration constant and x_0 the Debye length

$$x_0 = \sqrt{\frac{2\varepsilon kT}{q^2 p_0}}. \tag{9}$$

Writing that $p(0) = p_0$ leads to

$$x_1 = \frac{\arg\sinh gx_0}{g}. \tag{10}$$

Substitution of Eq. (10) in Eqs. (7) and (8) gives

$$F(x) = -\frac{2kT}{q} g \coth(gx + \arg\sinh gx_0), \tag{11}$$

$$p(x) = p_0 \left[\frac{gx_0}{\sinh(gx + \arg\sinh gx_0)}\right]^2. \tag{12}$$

The potential is obtained by integrating the electric field

$$V(x) = -\int_0^x F(x)dx = \frac{2kT}{q} \ln \frac{\sinh(gx + \arg\sinh gx_0)}{gx_0}. \tag{13}$$

Here, we assumed that $V = 0$ at the anode. The integration constant g can now be estimated by introducing the potential at the cathode, $V(d) = V_d$, where d is the thickness of the semiconductor and V_d the diffusion (or built-in) potential that equals the difference between the work functions of the anode and the cathode. At this stage, the calculation can no longer be performed by analysis and a numerical computation is used.

Figure 2 shows the calculated potential profiles of an organic diode with the following physical parameters: thickness of the semiconductor: 200 nm; anode work function: 4.8 eV; cathode work function: 4.2 eV; and ionization potential of the semiconductor: 4.9, 5.0, and 5.1 eV (to compare different injection barrier heights). In all cases, we assume that the LUMO level is sufficiently close to the vacuum level, so that no significant electron injection takes place.

From Fig. 2, we can say that the MIM model is completely valid as long as the anode barrier height is higher than about 0.2 eV. For smaller barrier heights, a slight band bending develops near the anode that tends to reduce the electric field in the bulk of the semiconductor. Note that the band bending appears at the "injecting" electrode, which is at variance with the Schottky model, where the band bending takes place near the "blocking electrode". We also note that, because of various interfacial effects discussed in detail elsewhere,[25] realistic metal-organic semiconductor junctions present an injection barrier in excess of ~0.3 eV, so that the MIM model could be applicable in most cases.

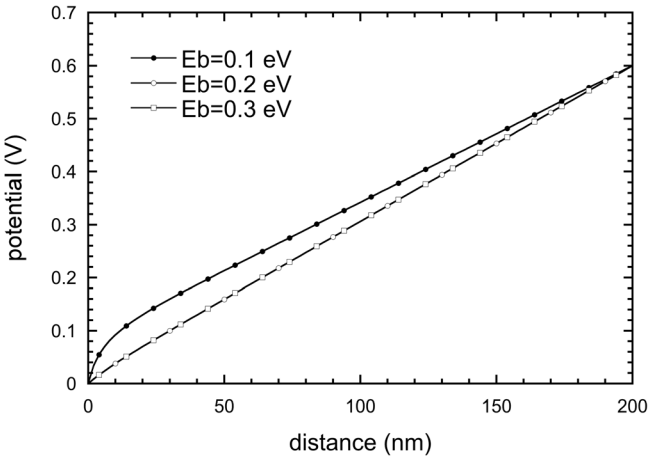

FIG. 2. Calculated potential profiles in a 200-nm-thick MIM diode with three values for the anode hole barrier: 0.1, 0.2, and 0.3 eV. The respective cathode barriers are 0.7, 0.8, and 0.9 eV.

2. Current-voltage model for the low-voltage regime

The exact analytical resolution of the general drift-diffusion Eq. (3) with finite current has been developed by Skinner[26] and Wright.[17] The solution involves Bessel functions, and even its asymptotic development does not lead to easy-to-handle analytical expressions. Instead, we develop here a simplified model directly inspired by the model of Shockley for the pn junction. One of the clearest physical descriptions of the concept can be found in the textbook of Ashcroft and Mermin.[20] At this point, it is worth mentioning that our model differs from that of the pn junction in that we only consider one kind of charge carrier; here, holes.

The basic idea is that the total current density j is the difference between two components: one originating from holes injected at the anode, j_{an}, and one from holes injected at the cathode, j_{cath}. As expected from Eq. (6) and Fig. 2, the density of holes at the anode is considerably higher than that at the cathode. However, Fig. 1 shows that, as long as the voltage applied to the anode (V_a) is lower than the diffusion potential, the electric field points against the hole current from the anode, so that only holes with high thermal energy can contribute to the anode current. Hence, the anode current is proportional to $e^{-q(V_d - V_a)/kT} \propto e^{qV_a/kT}$.

In contrast, at the cathode, the direction of the electric field favors the drift of (small number of) injected carriers. Thus, the cathode current is given by the elementary charge times the density of holes at the cathode, p_1, times their mobility, μ, times the electric field,

$$j_{cath} = qp_1\mu \frac{V_d - V_a}{d}. \tag{14}$$

At zero applied voltage, the total current is zero, so that

$$j_{an}(V_a = 0) = j_{cath}(V_a = 0). \tag{15}$$

Taking into account the voltage dependence of the anode current, we can write

$$j_{an} = j_{an}(V_a = 0)e^{qV_a/kT} = qp_1\mu\frac{V_d}{d}e^{qV_a/kT}. \quad (16)$$

Combining Eqs. (14) and (16) and the definition of p_1, we finally get

$$j = j_s\left(e^{qV_a/kT} - 1 + \frac{V_a}{V_d}\right), \quad (17)$$

$$j_s = q\mu\frac{V_d}{d}N_v e^{-E_b^{cath}/kT}. \quad (18)$$

Note that Eq. (17) differs from that of the pn junction by the third factor in the brackets at the right hand side that explains slight voltage dependence of the reverse current. At this stage, it is worth pointing out that the current is controlled by the electrode with the lowest hole injection (namely, the cathode). This operation mechanism reminds that of the pn junction, in which the current is controlled by minority carriers. At applied voltages higher than a few kT/q, Eq. (17) simplifies to

$$j = j_s e^{qV_a/kT}. \quad (19)$$

B. Effect of traps in the semiconductor

1. Defining a band edge in the presence of traps

Before analyzing the effect of traps on the diode, let us first recall how a band edge can be defined in a disordered semiconductor and how a distinction can be made between "valence" (or "conduction") and "trap" states. A first useful concept is the mobility edge (ME)[27,28] that was first developed for amorphous inorganic semiconductors. The ME separates extended from localized states. The existence of the former arises from the similarity of the short range configuration in the amorphous solid to its crystalline analogy. Transport in localized states occurs through hopping and is expected to be negligible in comparison with that in the extended states; hence, we see an abrupt increase in mobility at the ME. Only charge carriers that are thermally activated to states above the ME contribute to charge transport. This constitutes the base of the well-documented multiple trapping and release (MTR) model.

However, the presence of extended states is unlikely in disordered organic semiconductors. Instead, the valence and conduction bands are described in terms of a Gaussian distribution of localized states. In such a case, the transport energy (TE) is a more relevant concept.[29] TE is a particular temperature-dependent energy level within the band tail that was first coined by Grunewald and Thomas[30] from a numerical analysis of the equilibrium hopping conductivity. As shown later by Monroe,[31] an electron starting from an upper energy level of the distribution makes a series of hops downward in energy until it reaches some particular energy (TE), at which the relaxation process changes drastically. Near and below this TE, the transport resembles the MTR process, with the ME replaced by the TE. Accordingly, we will consider the TE as the band edge in the following discussions.

2. Diode with traps at thermal equilibrium

The presence of a distribution of traps in organic semiconductors is now well documented.[11,12,32] The most appropriate model for small molecules is the exponential DOS,

$$N(E) = \frac{N_t}{kT_c}e^{-(E-E_v)/kT_c}, \quad (20)$$

where E_v is the energy of the valence band edge, N_t the total density of traps, and T_c a characteristic temperature connected to the width of the distribution. The density of trapped holes is estimated by integrating this DOS times the Fermi-Dirac distribution (for holes) over the available energy range,

$$p_t(E_F) = \int_{-\infty}^{+\infty}\frac{N(E)\mathrm{d}E}{1 + e^{-(E-E_F+qV)/kT}}. \quad (21)$$

Here, E_F is the Fermi energy at equilibrium. Because $T_c > T$ in general, the DOS in Eq. (20) is slowly varying function with energy compared to the Fermi function, so that the latter can be approximated to a step function, thus yielding the following relation between the density of trapped holes and the potential:

$$p_t = p_{t0}e^{-qV/kT_c}, \quad (22)$$

where $p_{t0} = N_t e^{-E_b/kT_c}$ is the value of p_t at $x = 0$. From Eqs. (6) and (22), the ratio between free and trapped holes is given by

$$\frac{p}{N_v} = \left(\frac{p_t}{N_t}\right)^{T_c/T}. \quad (23)$$

The potential profile can now be calculated by replacing p by $p + p_t$ in Poisson's equation in Eq. (1). However, generally $p_t \gg p$, so that a valid Poisson's equation can be simply obtained by replacing p by p_t in Eq. (1). On the other hand, the drift-diffusion equation must be left unchanged because only "free" carriers can participate in the charge transport. Making use of Eqs. (1) and (23), Eq. (3) becomes, after several manipulations,

$$j = qN_v\mu\left(\frac{\varepsilon}{qN_t}\right)^l\left(\frac{\mathrm{d}F}{\mathrm{d}x}\right)^{l-1}\left(F\frac{\mathrm{d}F}{\mathrm{d}x} - \frac{kT_c}{q}\frac{\mathrm{d}^2F}{\mathrm{d}x^2}\right), \quad (24)$$

where $l = T_c/T$. At equilibrium, Eq. (24) reduces to Eq. (4), with T_c instead of T. Accordingly, the solution for $V(x)$ is obtained by changing T to T_c and p_0 to p_{t0}. Figure 3 compares the potential profile of a diode without and with traps with the parameters listed in Table I. Here, the trap density and characteristic temperature are representative values close to the experimentally extracted trap parameters in Sec. IV B. Note that these values differ from those deduced in a recent study from pentacene-based organic field-effect transistors.[32] The difference can mainly arise from the direction of current flow; the current flows across the film in a diode, whereas it flows along the film in a transistor. It could also come from the already mentioned very different charge carrier density involved in both devices.

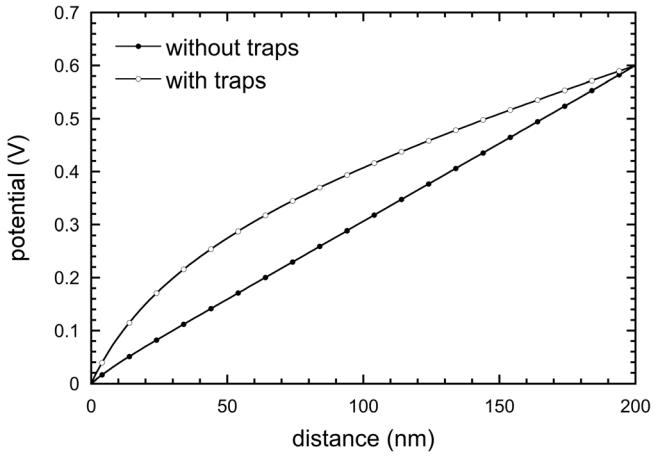

FIG. 3. Calculated potential profiles in an MIM diode without and with a distribution of traps. The parameters used for the calculation are listed in Table I.

The effect of the distribution of traps is globally identical to the lowering of injection barrier from the anode. Physically, traps provide available states that can be filled by injected carriers from the anode. These trapped (or fixed) carriers give rise to a screening effect that bends the band. In turn, the band bending can be viewed as a reduction of potential difference between the anode and the cathode. This point will be discussed in more detail in Sec. III B with simulated voltage-dependent band structures.

3. Bulk-limited current with exponential trap distribution

As indicated in Fig. 1, when the forward voltage exceeds the built-in voltage, the current is no longer limited by charge injection but limited by the bulk property of the semiconductor. This is because the direction of electric field now favors the drift contribution of injected carriers at the "anode". If the semiconductor does not contain any traps (corresponding to the arguments in Sec. II A), the bulk current follows the well-known Mott-Gurney relation (space-charge limited current (SCLC)) and the current is a quadratic function of voltage.[14,33]

When the bulk current is affected by exponentially distributed traps, one can refer to the classical model of Mark and Helfrich,[34] which predicts the current-voltage relation of the form

TABLE I. Parameters used for the analytical calculations.

Parameter	Value
Effective density of states N_v (cm^{-3})	10^{20}
Ionization potential IP (eV)	5.1
Anode work function W_m^{an} (eV)	4.8
Cathode work function W_m^{cath} (eV)	4.2
Temperature (K)	300
Dielectric constant	3.6
Total trap density N_t (cm^{-3})	2×10^{18}
Characteristic temperature T_c (K)	1200

$$j = qN_v\mu\left(\frac{\varepsilon}{qN_t}\frac{l}{l+1}\right)^l\left(\frac{2l+1}{l+1}\right)^{l+1}\frac{(V_a-V_d)^{l+1}}{d^{2l+1}}. \quad (25)$$

The foremost feature of Eq. (25) is that it predicts a power law shape in the current-voltage curve. Traditionally, the current is plotted in log-log coordinates, and the slope of the straight line $(l+1)$ is used as a direct access to the characteristic temperature (T_c) of the trap distribution.

As a final remark of this section on the trap studies in organic diodes, we emphasize that, up to this time, there was no dedicated study for the trap effect on the "low-voltage regime". Based on the trap-induced band bending effect modeled in this section, and by making use of the device simulation with the experimental application of Mark-Helfrich law, we will prove in Secs. III and IV that traps result in a significant ideality factor (decreased slope in the exponential current) at a low-voltage regime.

III. NUMERICAL SIMULATION

In this section, we present several results of a physically based two-dimensional simulation as a validation and extension tool of the analytical model. They will provide complementary data to the model, as the simulation gives exact numerical solutions for the system that cannot be analytically estimated (especially, calculation out of thermal equilibrium condition). We used the ATLAS simulator by SILVACO[35] for the organic diode simulation. This finite-element simulation solves a set of coupled Poisson's, continuity, and drift-diffusion equations and produces self-consistent solutions within a user-defined two-dimensional structure. We defined a metal-semiconductor-metal structure with 200 nm of pentacene (predefined material model in ATLAS) as an organic semiconductor.

A. Validity of the model

In Fig. 4, the simulated current-voltage $(j-V)$ curve is drawn together with that of the low-voltage analytical model developed in Sec. II A. The parameters for both curves are those listed in Table I, with hole mobility of pentacene as $0.15\ cm^2/V\cdot s$.[36] The simulated curve displays three distinct regimes introduced in Fig. 1: reverse, injection-limited, and

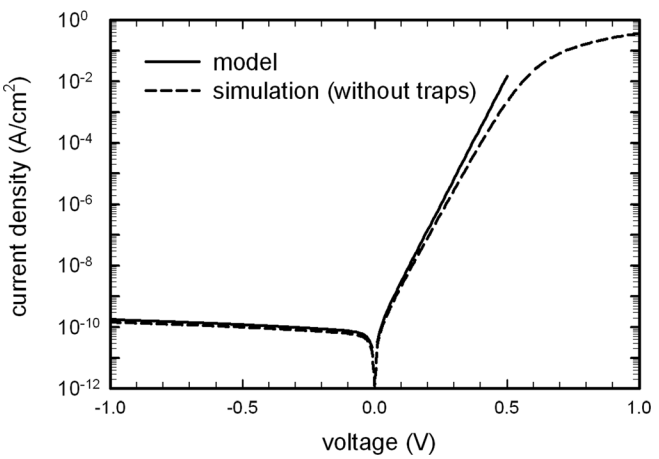

FIG. 4. Comparison between the simulated and analytical $j-V$ curves.

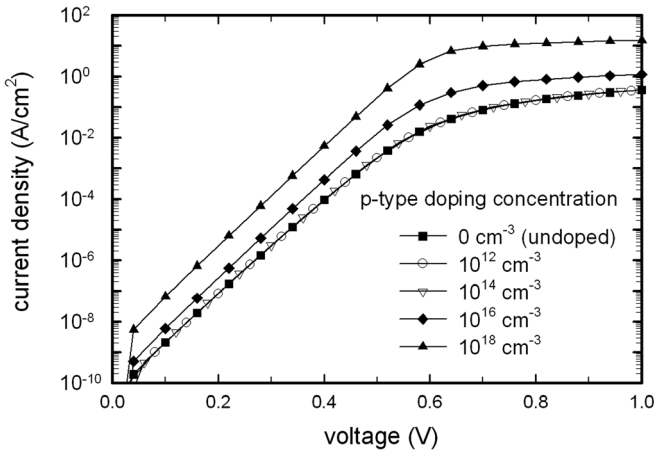

FIG. 5. Simulated $j - V$ curves with various doping concentrations in pentacene. This result points out that the assumption of zero doping is applicable as long as the dopant density lies below the injected carrier density at the anode.

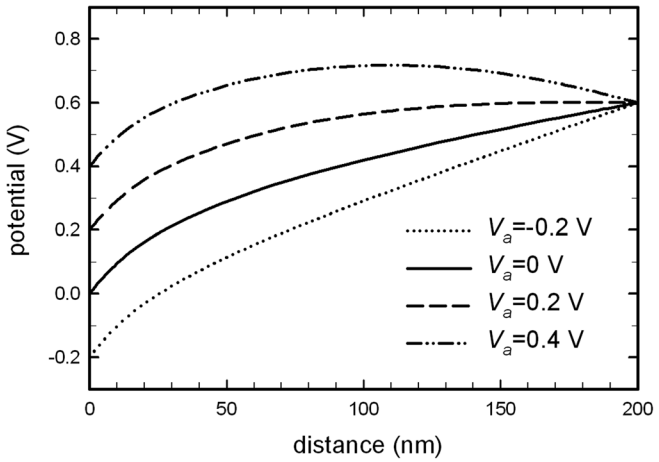

FIG. 6. Effect of an exponential trap distribution on the potential profile as estimated by simulation with the same parameters as for the analytical model in Fig. 3.

bulk-limited. Under reverse-bias ($V_a < 0$), both curves show slightly increasing reverse-current, as predicted by our model. In the injection-limited forward-bias regime ($0 < V_a < V_d$) (main focus of this study), the analytical curve fairly matches the simulation, apart from small deviation as approaching the bulk regime. The third regime (bulk-limited forward-bias regime) is not traced by the low-voltage model. The simulation indicates that, in this regime, the current is no longer exponential with voltage; rather, it starts following a power-law dependence (SCLC prevails here).

All that has been developed until this point is strongly based on the primary assumption that the organic semiconductor is strictly undoped, so that only injected charges govern the current flow in the diode. In order to solidify this hypothesis, a series of simulations with increasing doping concentration has been conducted. Figure 5 shows the forward $j - V$ characteristics from zero to the heavily doped case. Obviously, doping up to 10^{14} cm^{-3} does not influence the current, because the injected carriers are more abundant than those generated by dopants. It is only when the doping concentration becomes higher than 10^{16} cm^{-3} that the current significantly raises, owing to additional free carriers. Accordingly, the organic semiconductor can be safely described as undoped in realistic cases, even though small amounts of unintentional dopants could exist in fabricated devices.

B. Trap-induced ideality factor

Figure 6 presents the simulated potential profiles with an exponential distribution of traps. With the parameters listed in Table I, the simulated potential profile at thermal equilibrium ($V_a = 0$) matches well that calculated by the model (see Fig. 3); band bending occurs at the injecting interface due to the trapped (fixed) charges. Then, the simulation also allows us to monitor the variation of the profiles as varying applied V_a, which is, in fact, a key element to understand the trap-induced ideality factor.

The influence of traps on the $j - V$ characteristics of the organic diode is shown in Fig. 7 and can be discussed as follows: First, there is no significant change in the reverse-bias regime, because the reverse current is dominated by the drift contribution of the free carriers injected at the cathode. Next, in the injection-limited regime (from 0 V to roughly 0.5 V), we clearly observe a decrease of the slope, which can be interpreted in terms of an ideality factor n. Third, the bulk-limited current (above 0.5 V) is considerably lowered, as predicted by Mark-Helfrich's model in Eq. (25). The origin of the trap-induced ideality factor can be elucidated from the potential profiles in Fig. 6. The effect of traps on the potential profile can be viewed as a reduction of the injection barrier at the anode. If we define the reduction as ΔV ($\Delta V > 0$), the current is no longer proportional to $e^{qV_a/kT}$, but rather to $e^{q(V_a-\Delta V)/kT}$. Generally, ΔV depends on the applied voltage (as shown in Fig. 6). A first order development of ΔV with V_a leads to $\Delta V \simeq \alpha V_a$ and

$$j = j_s e^{qV_a/nkT}, \tag{26}$$

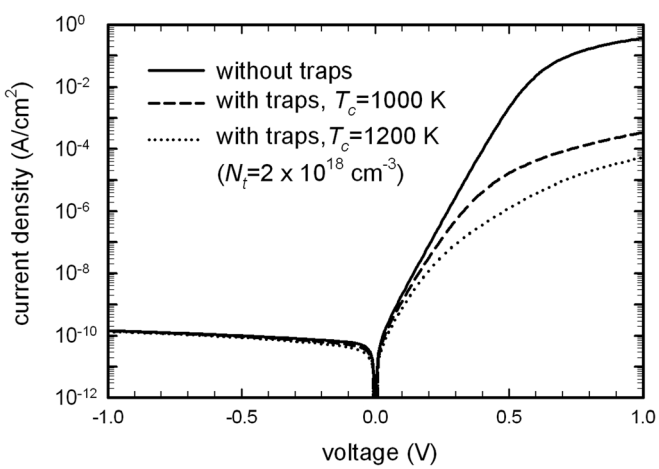

FIG. 7. Effect of an exponential distribution of traps on the $j - V$ characteristics of an organic diode. The traps result in a deviation of the forward current at low biases from the exponential growth, which can be interpreted in terms of an ideality factor. Ideality factor becomes higher with increasing T_c.

where $n = 1/(1-\alpha)$ is the ideality factor. However, it should be noted that Eq. (26) looks oversimplified when the current is strongly limited by traps. In that case, the current is not perfectly linear with V_a in the semi-log plot (see $T_c = 1200$ K curve in Fig. 7). In other words, a first order approximation is less reliable in such a situation.

There were many experimental reports showing considerable ideality factor in organic diodes. Haldi *et al.*,[37] for instance, studied single-layer diodes with various organic semiconductors and measured ideality factors ranged from 1.6 to 4.3. No clear physical explanation, however, has been put forward yet. We believe that our result is the first and most relevant description for the origin of the ideality factor in organic diodes.

IV. EXPERIMENTAL PROOF

This section deals with an experimental analysis on the pentacene-based organic diode, which supports the explanation for the trap-induced ideality factor in Secs. II B and III B. If an organic diode with single crystalline semiconductor or low-defect material is under investigation, the ideality factor could be close to unity and show trap-free behavior (Secs. II A and III A). Evaporated pentacene film is known for its polycrystalline phase, and grain (or domain) boundaries mainly contain trapping sites.[13,38] It is thus expected that pentacene diode could be a useful test device concerning trap effects. We could extract actual trap parameters (N_t and T_c) by applying Eq. (25) to the bulk-regime current of our device. Incorporating this exact information on traps, the simulation could reproduce the measured $j-V$ curve at low-voltage regime with satisfying precision for the ideality factor.

A. Fabrication: Pentacene diode

Pentacene-based organic diodes were fabricated with metal/semiconductor/metal structure. Au (anode), pentacene (organic semiconductor), and Al (cathode) were subsequently evaporated on a cleaned glass substrate. All evaporation processes were done under a vacuum pressure of about 2×10^{-7} mbar, with the substrate kept at room temperature. The evaporation rate of pentacene was 0.1 nm/sec with a final thickness of 200 nm. $j-V$ measurements were carried out using a semiconductor characterization system (Keithley 4200) in dark under nitrogen atmosphere. The devices are transferred into the measurement system right after the fabrication process without exposure to the ambient air. This experimental setup minimizes contamination or degradation by chemical reaction with ambient gas molecules.

B. Bulk-limited current: Evidence for traps

Figure 8 shows the measured bulk-limited current in log-log scale. The reasonable linearity of the measured curve ascertains a power-law relationship between current and voltage. The estimated slope of the curve is 5.4, and it means that the current is strongly limited by traps.[34] This value can be directly converted to $l = 4.4$ and $T_c = 1320$ K. The total density of traps N_t was then obtained by optimizing

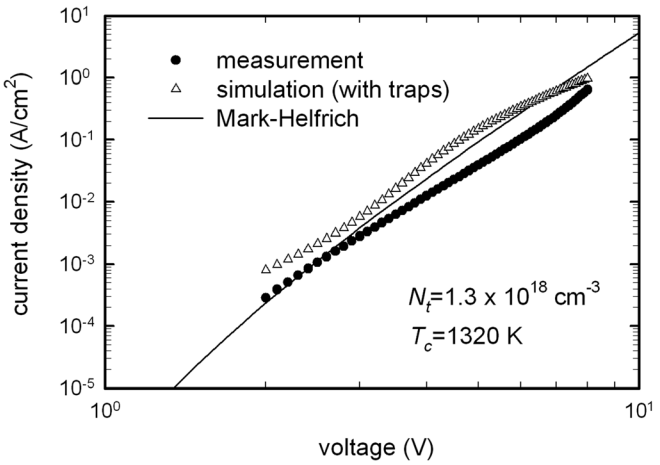

FIG. 8. $j-V$ data in the bulk-limited regime (2 to 8 V) plotted in log-log scale together with the best-fit simulation and the prediction of Mark-Helfrich's model (trap-limited SCLC).

the measured data to the simulation, resulting in $N_t = 1.3 \times 10^{18}\,\mathrm{cm}^{-3}$. The curve calculated with the Mark-Helfrich model [Eq. (25)] with extracted N_t and T_c is plotted in Fig. 8 as well. Note that, because we inserted $V_a - V_d$ (instead of V_a) as the voltage term in Eq. (25) to correct for the asymmetric electrodes, the curve is not perfectly linear, but slightly bends downward when approaching V_d.

C. Low-voltage regime: Ideality factor

The measured low-voltage regime current is shown in Fig. 9. It also exhibits three-regime behavior with increasing reverse-current and exponential injection-current. A linear regression gives an approximate ideality factor n of 2.1 in the pentacene diode. With fixed trap parameters ($N_t = 1.3 \times 10^{18}\,\mathrm{cm}^{-3}$ and $T_c = 1320$ K), we could fit the low-voltage regime curve to extract injection barrier heights; it should be kept in mind that the current in this regime strongly (exponentially) depends on the cathode barrier as predicted by our model [Eqs. (17) and (18)]. Assuming an

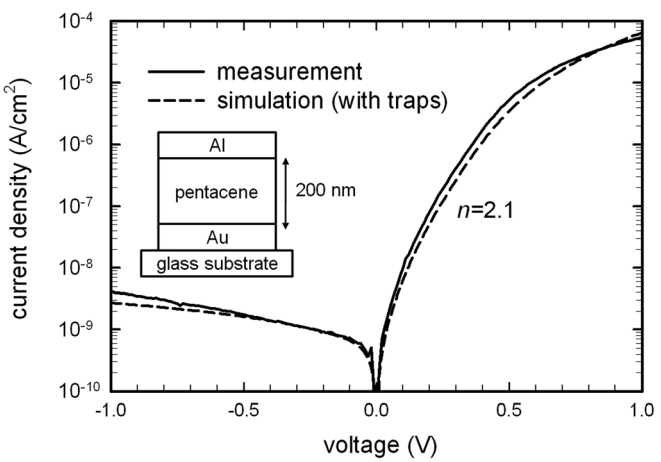

FIG. 9. Measured $j-V$ curve of a pentacene diode. The inset shows the structure on a glass substrate. The Au bottom electrode serves as the injecting contact (anode), and the Al top electrode is the blocking contact (cathode). The active area of the device is 4×10^{-4} cm^2. The best simulation is also shown.

ionization potential *IP* of pentacene as 5.2 eV, the work functions of the Au anode and Al cathode were extracted to be 4.9 and 4.38 eV, respectively. They correspond to the anode barrier of 0.3 eV and the cathode barrier of 0.82 eV. Figure 9 shows a nice agreement between the optimized simulation and the experimental data; we can successfully account for the emergence of the ideality factor by bulk traps in the organic semiconductor. In addition, the simulated $j-V$ curve also shows the same ideality factor of ~2.1.

V. CONCLUSION

In the present work, we revisit the physics of the single-layer organic diode. We introduce a new simple analytical model for the low-voltage regime of the diode, an area of great interest for organic photovoltaic cells. We show that the current at applied voltage lower than the diffusion potential results from the balance between the charge carriers injected from both electrodes, a mechanism that strongly reminds that of the pn junction. Such a description is at variance with the most often invoked picture of the conventional Schottky diode, in which the current is governed by the interface between the semiconductor and the blocking electrode. The effect of traps is to reduce the overall current of the diode, and they also induce a substantial ideality factor. We provide two-dimensional physically based finite element simulation in order to validate the model. The current-voltage characteristics given by the analytical model are in good agreement with the simulation results. Another appealing aspect of our model is that it provides a physical meaning to basic parameters, such as the saturation current, which could be utilized within the frame of organic circuit compact modeling. We are currently working on the extension of the present model to the case of heterojunction organic photovoltaic cells.

ACKNOWLEDGMENTS

This work has been supported by NoE PolyNet from the European Community's Seventh Framework Program (FP7/2007–2013) under Grant No. 214006. C.H. Kim wishes to thank the Vice Presidency for External Relations (DRE) in Ecole Polytechnique for the Ph.D. fellowship.

[1]B. Geffroy, P. L. Roy, and C. Prat, Polym. Int. **55**, 572 (2006).
[2]K. T. Kamtekar, A. P. Monkman, and M. R. Bryce, Adv. Mater. **22**, 572 (2010).
[3]C. Brabec, U. Scherf, and V. Dyakonov, *Organic Photovoltaics: Materials, Device Physics, and Manufacturing Technologies* (Wiley-VCH, Weinheim, 2008).
[4]M. J. Currie, J. K. Mapel, T. D. Heidel, S. Goffri, and M. A. Baldo, Science **321**, 226 (2008).
[5]M. C. Scharber, D. Wuhlbacher, M. Koppe, P. Denk, C. Waldauf, A. J. Heeger, and C. L. Brabec, Adv. Mater. **18**, 789 (2006).
[6]B. Crone, P. Davids, I. Campbell, and D. Smith, J. Appl. Phys. **84**, 833 (1998).
[7]K. Vandewal, K. Tvingstedt, A. Gadisa, O. Inganas, and J. V. Manca, Nature Mater. **8**, 904 (2009).
[8]A. Moliton and J.-M. Nunzi, Polym. Int. **55**, 583 (2006).
[9]L. J. A. Koster, E. C. P. Smits, V. D. Mihailetchi, and P. W. M. Blom, Phys. Rev. B **72**, 085205 (2005).
[10]C. H. Kim, O. Yaghmazadeh, D. Tondelier, Y. B. Jeong, Y. Bonnassieux, and G. Horowitz, J. Appl. Phys. **109**, 083710 (2011).
[11]V. Kumar, S. Jain, A. Kapoor, J. Poortmans, and R. Mertens, J. Appl. Phys. **94**, 1283 (2003).
[12]A. Salleo, T. W. Chen, A. R. Volkel, Y. Wu, P. Liu, B. S. Ong, and R. A. Street, Phys. Rev. B **70**, 115311 (2004).
[13]W. L. Kalb, S. Haas, C. Krellner, T. Mathis, and B. Batlogg, Phys. Rev. B **81**, 115315 (2010).
[14]N. F. Mott and R. W. Gurney, *Electronic Processes in Ionic Crystals*, 2nd ed. (Oxford University Press, Oxford, 1940).
[15]A. Rose, Phys. Rev. **97**, 1538 (1955).
[16]M. A. Lampert, Phys. Rev. **103**, 1648 (1956).
[17]G. T. Wright, Solid-State Electron. **2**, 165 (1961).
[18]D. J. Page, Solid-State Electron. **9**, 255 (1966).
[19]C. Tanase, E. J. Meijer, P. W. M. Blom, and D. M. de Leeuw, Phys. Rev. Lett. **91**, 216601 (2003).
[20]N. W. Ashcroft and N. D. Mermin, *Solid State Physics* (Holt, Rinehart and Winston, New York, 1976).
[21]Y. Roichman and N. Tessler, Appl. Phys. Lett. **80**, 1948 (2002).
[22]Y.-Q. Peng, J.-H. Yang, and F.-P. Lu, Appl. Phys. A: Mater. Sci. Process. **83**, 305 (2006).
[23]A. Das and A. Khan, Appl. Phys. A: Mater. Sci. Process. **93**, 527 (2008).
[24]S. M. Skinner, J. Appl. Phys. **26**, 498 (1955).
[25]J. Hwang, A. Wan, and A. Kahn, Mater. Sci. Eng. R **64**, 1 (2009).
[26]S. M. Skinner, J. Appl. Phys. **26**, 509 (1955).
[27]P. W. Anderson, Proc. Natl. Acad. Sci. U. S. A. **69**, 1097 (1972).
[28]J. M. Marshall, Rep. Prog. Phys. **46**, 1235 (1983).
[29]S. D. Baranovskii, O. Rubel, and P. Thomas, Thin Solid Films **487**, 2 (2005).
[30]M. Grunewald and P. Thomas, Phys. Status Solidi B **94**, 125 (1979).
[31]D. Monroe, Phys. Rev. Lett. **54**, 146 (1985).
[32]W. L. Kalb and B. Batlogg, Phys. Rev. B **81**, 035327 (2010).
[33]D. Braga, N. Battaglini, A. Yassar, G. Horowitz, M. Campione, A. Sassella, and A. Borghesi, Phys. Rev. B **77**, 115205 (2008).
[34]P. Mark and W. Helfrich, J. Appl. Phys. **33**, 205 (1962).
[35]See http://www.silvaco.com for information about Silvaco Data Systems Inc.
[36]S. Steudel, K. Myny, V. Arkhipov, C. Deibel, S. De Vusser, J. Genoe, and P. Heremans, Nature Mater. **4**, 597 (2005).
[37]A. Haldi, A. Sharma, W. J. Potscavage, and B. Kippelen, J. Appl. Phys. **104**, 064503 (2008).
[38]S. Verlaak, V. Arkhipov, and P. Heremans, Appl. Phys. Lett. **82**, 745 (2003).